COMADEM

International Journal of Condition Monitoring and Diagnostic Engineering Management

Experimental and Numerical Study of Local Scouring Downstream of D-Type Piano Key Weir

Fariba Ahmadi Dehrashid 1[a], Saeed Gohari 2[a] *, Taimoor Asim 3[b], Rakesh Mishra 4[c], Alireza Khoshkonesh 5[a], Farhad Bahmanpouri 6[d], and Blaise Nsom 7[e]

[a] *Department of Water Science and Engineering, University of Bu Ali Sina, 65178 Hamedan, Iran*
[b] *Robert Gordon University, Garthdee Roa, AB10 7GJ ABERDEEN, United Kingdom*
[c] *School of Computing and Engineering University of Huddersfield,, HD1 3DH HUDDERSFIELD, United Kingdom*
[d] *Architectural and Environmental Engineering Department (DICEA), University of Naples Federico II (UNINA), 80125 Napoli NA, Italy*
[e] *Université de Bretagne Occidentale. IRDL/UBO UMR CNRS 6027. Rue de Kergoat, 29285 Brest, France*

∗ *Corresponding author. Tel.: +98-912-633-5291; email: s.gohari@basu.ac.ir*

ABSTRACT

The present paper aims to evaluate the local scouring of non-cohesive sediment beds consisted of uniform sediment particles downstream of a D - type piano key weir in steady flow condition. The experiments were conducted for one model of D - type piano key weir with five keys. Accordingly, the effect of hydraulic parameters was examined on scouring profiles and depth, downstream of the piano key weir. While nine runs were conducted to evaluate the local scouring downstream of the piano key weir under clear-water conditions with different discharge rates and tail water depths. The experimental results showed that the maximum scouring depth increased with increasing the discharge. Further, increasing the tail water depth resulted in decreasing the largest scour depth. The 3D numerical simulation was implemented using a CFD package. Overall, the results of the numerical modelling were in agreement with the experimental data.

Keywords: *Piano key weir (PKW) ; Local scour ; Non-cohesive sediment ; Computation fluid dynamics(CFD) ; Volume of fluid (VOF) .*
Article history: *Received ; Published .*

1. Introduction

The piano key weir (PKW) is an improvement of the labyrinth weirs. The advantages of PKW are higher safety-factor of dams and high economic efficiency. Further, the PKWs have a low retention cost, higher reservoir storage volume and the flood control system (Falvey, 2003; Lempérière et al., 2003,2011; Machiels et al., 2011; Kabiri-Samani and Javaheri, 2012; Ribeiro et al., 2012; Mehboudi et al. 2016; Karimi et al., 2019).

The foundation stability of hydraulic structures may decay because of the downstream local scour due to the flow taking place in the form of turbulent water jets. Generally, the complete protection against scouring is often impossible and expensive. Therefore, understanding the scouring mechanism downstream the PKWs is crucial in terms of finding suitable solutions and ways to control the scouring process and mitigate the risk of destruction.

Local scouring downstream of the hydraulic structures within a steady flow condition have been extensively studied before. Rajaratnam and Macdougall (1983) based upon experimental study indicated that there was no significant increase in bed erosion after about 30 min during the scouring induced by plane turbulent jets. Accordingly, scouring profiles were evaluated to study geometric characteristics independent of time and sediment size (Rajaratnam 1981; Balachandar 1997; Yang et al. 2020). Kumar and Ahmad (2020) pointed out the impacts of sediment size and tail water depth on the scour depth downstream of a spillway apron. Dey and Sarkar (2005-2007) addressed shifts in the characteristic lengths of a scour hole downstream of an apron based upon the particle Froude number for sediments with uniform and non-uniform gradations. The results of their experiments revealed that all the parameters of the scour hole, such as the maximum scour depth and the dune height, were augmented by increasing the leakage rate. Faruque et al. (2006) scrutinized the effect of submergence on scouring processes by using a square cross-section nozzle on a non-cohesive sand bed, due to three-dimensional jet authorization. Results showed that the tail water depth, particle Froude number, and the ratio of grain size-to nozzle size had a significant impact on the width of the scour hole. Further, the maximum scouring depth was not deeper at the lower range of submergence, however, the larger depth of scouring corresponded to higher tail water depths. Pagliara et al. (2006) studied a single jet on a horizontal sediment bed that produced a 3D scour hole based on the different sediment combinations, the jet aeration, the angle of jet impact, and the tail water depth. Bhuiyan et al. (2007) evaluated the effect of a W-type weir (without an apron) on the downstream processes of sediment transportation, especially the scour hole formation. A short distance downstream of the weir was measured that corresponded to the maximum scour depth, irrespective of the boundary conditions. Jüstrich et al. (2016) scrutinized the scouring process downstream of an A-type piano key weir and demonstrated that

the greatest slope of the scour depth at the downstream of the piano key weir was affected by the static angle of the substrate material. Further, the dimensions of the local scour in the piano key weir were very similar to the scour in jet-like flows.

Despite many studies on local scouring downstream of the hydraulic structures, detailed experimental and numerical studies focusing on the scouring mechanism downstream of the piano key weirs are scarce (Jüstrich et al., 2016; Kumar and Ahmad, 2020). Therefore, in the present study, local scouring morpho-dynamic features including the scour hole profiles and depth were scrutinized both quantitatively and qualitatively.

The present study aims to evaluate the scouring processes based on experimental and numerical modeling. The experimental runs were conducted to evaluate the local scouring downstream a D - type piano key weir under clear-water and steady flow conditions with different discharges and tail water depths. The numerical modeling was implemented by coupling the volume of fluid (VOF) with a series of sediment scours and bed load transport formulas in a 3D modeling framework using Flow-3D software.

2. Problem statement

There are four major types of PKWs which are classified as with and without overhangs as A-D (Fig. 1). In the present study, the inflow discharge rate and the tail water depth were considered as independent variables in evaluating the local scouring downstream a D-type piano key weir. The experimental data were used for validating the numerical simulations. The free surface steady flow was modeled using VOF method while the sediment entrainment, scouring and bed load transport processes were simulated through the transport equations in CFD package. The VOF method has been shown to have good accuracy as compared to other numerical methods used for evaluating the free surface flows (Flow Science 2010, Li et al. 2019a, 2019b, Khoshkonesh et al. 2019, Nsom et al. (2019), Bahmanpouri et al. 2020). In this investigation, the turbulence features were captured through the large eddy simulation (LES) model after comparing the efficiency of various turbulence models in reproducing the bed deformations.

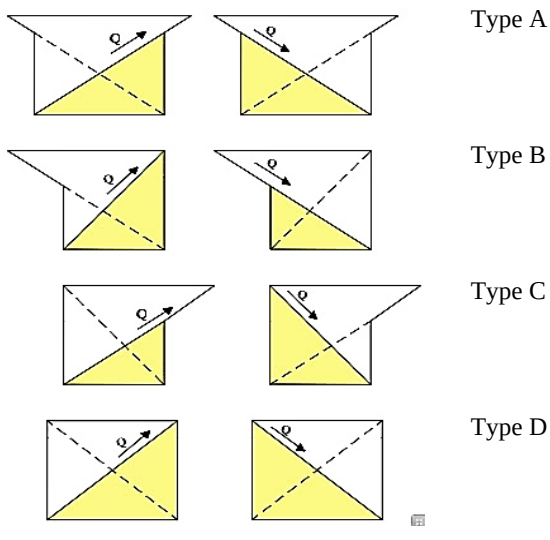

Figure 1. Various types of PKWs (Kabiri-Samani and Javaheri, 2012; Karimi et al., 2019)

3. Experimental set-up

The experiments were conducted in the hydraulic laboratory of Bu-Ali Sina University. A standard flume was made from galvanized iron and the glass walls having the following dimensions.:

Length 10 m long,

Width 0.5 m wide,

Height 0.5 m high

The figure 2 shows the dimensional details of the flume. The flume is raised to 1.3 m from the laboratory floor with a constant bed slope of 0.001. The range of discharge rates Q was chosen between 10 to 20 l/s considering the pump capacity and normal flow conditions. To measure the discharge rate, a calibrated triangular weir (error of 0.1 l/s) with a 90° angle was employed at the end of the flume. The discharge rate was controlled by a calibrated flow-meter mounted on the inlet flow pipe. Further, the tail water depth was adjusted by a sluice gate at the end of the flume.

In the present study, a *D* - type piano key weir model with 5 keys (3 input key and 2 output keys) with dimension of $B = 0.4$ m, $W = 0.5$ m, $P = 0.2$ m, $w_i = w_o = 0.1$ m and $s_i = s_o = 0.5$ was employed (B: weir length, W: weir width, P: weir height, w_i and w_o: width of the inlet and outlet keys, s_i and s_o: the slope of the inlet and outlet keys).

A schematic view of the weir is shown in Fig. 3. The downstream of the weir, a rigid apron with 0.6 m long, 0.5 m width, and 0.17 m height was employed. The length of the apron was determined based on the jump length criterion. In this direction, the length of the apron was equal to 1.5 times the hydraulic jump length (Bradley and Peterka, 1957; Kumar and Ahmad, 2020). The erodible bed consisted of sediment particles filled to 0.17 m depth and 2.1 m long. Sand particles with a median grain size of d_{50} = 1 mm and a uniformity coefficient of $\sigma_g = \sqrt{\frac{d_{84}}{d_{16}}} = 1.3$ was employed in the experiments. The sediment particles density, the angle of repose and Manning-Strickler roughness were equal $\rho_s = 2.65$, $\varphi = 33°$, $n = 0.015$ respectively.

Nine experimental runs were conducted under different steady-inflow conditions as listed in Table. 1. While the Reynolds number was higher than 10^4 and the Froude number was lower than 1, the flow regime was subcritical and turbulent. Every test condition was kept constant for 9 hours (equilibrium time). For each run, once no sand particle were observed that were removed from the scour's hole and transferred downstream, the pump was stopped and that time was considered as end time.

The scour depth after 9 hours reached a constant magnitude i.e. almost no change was noticed after this time, and the scour depth reached a relative equilibrium (Fig. 4). Therefore, the 9 hours run time was considered as the equilibrium time for all tests. After finishing each test, the water in the flume was drained out and bed topography was measured in a square grid of size 2cm * 2cm using a point gauge (La ica 810K model) with a travel accuracy of ±1 mm.

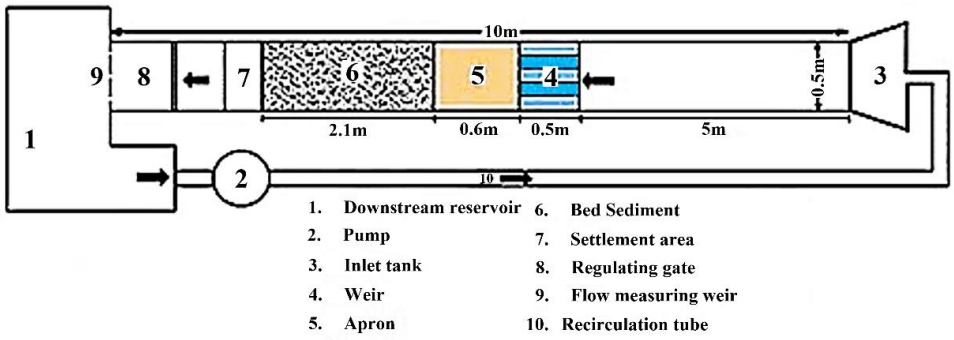

Figure 2. Experimental flume scheme

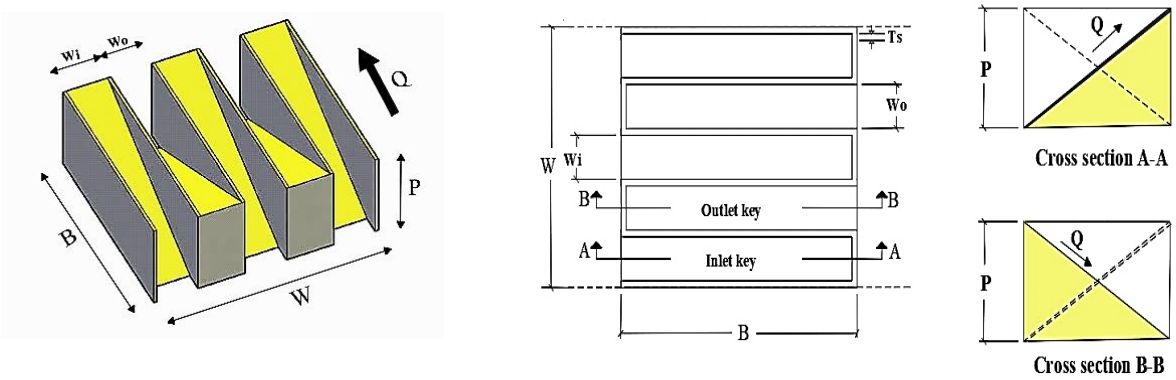

(a) **(b)**

Figure 3. (a) 3D schematic (b) the scheme of plan and cross-sections of D-Type PKW

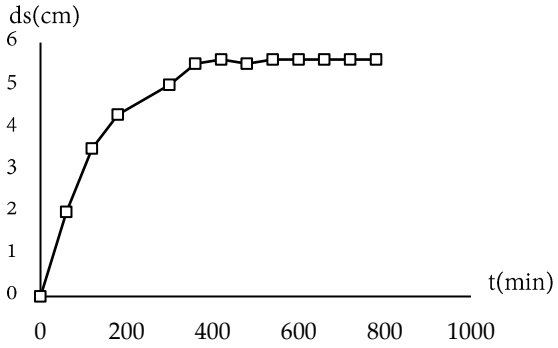

Figure 4. Variations of scour depth against time for the sample run

Table 1. Experimental tests parameters

Case	Weir type	Discharge Q (m^3/s)	Mean velocity U (m/s)	Reservoir Depth Y_u (cm)	Tail water depth Y_t (cm)	The depth top of the weir crest H_u (cm)	Sediment depth d_s (m)	Critical Shields number θ_{cr}	Reynolds number Re	Froude number Fr	Particle Froude number Fr_d
1	D-type PKW5	0.01	0.25	37.3	5	1.2	0.17	0.04	12568.74	0.362	2
2		0.01	0.33	37.2	8	1.1	0.17	0.04	19734.44	0.367	2.6
3		0.01	0.36	37.1	10	1.2	0.17	0.04	25950.54	0.366	2.9
4		0.015	0.3	38.8	7	1.7	0.17	0.04	16628.29	0.366	2.4
5		0.015	0.34	38.8	8.5	1.8	0.17	0.04	21292.18	0.367	2.6
6		0.015	0.36	38.5	10	1.5	0.17	0.04	25950.54	0.366	2.9
7		0.02	0.36	39.6	10	2.5	0.17	0.04	25950.54	0.366	2.9
8		0.02	0.4	39.5	12	2.5	0.17	0.05	32054.48	0.364	3.1
9		0.02	0.42	39.3	13.5	2.3	0.17	0.05	36506.96	0.361	3.3

3.1. Dimensional Analysis

For clear water condition the scour depth downstream of D - type PKW is a function of the following parameters:

$$\mathrm{f}(q.Y_t.H.P.N.B.W_i.W_o.W.S_i.S_o.L_b.T.\rho_w.\rho_s.\ g.\mu.\sigma_g.d_{50}.d_s.L_s.L_o.h_d.L_d) = 0 \quad (1)$$

Where q : the weir discharge per unit width, Y_t: tail water depth, H: the water depth at top of the weir crest, P: weir height, N: number of keys, B: weir length, W_i and W_o: width of inlet and outlet keys respectively, W: weir width, S_i and S_o: slope of inlet and outlet keys, respectively, L_b: apron length, T: equilibrium time, ρ_w: density of water, ρ_s: density of sediment, g: gravity acceleration, μ: dynamic fluid viscosity, σ_g: uniformity coefficient, d_{50}: median grain size, d_s: largest scour depth, L_s: distance to maximum scour position, L_o: length of scour hole, h_d : dune height, . L_d: length to dune crest. Since the purpose of this study was to evaluate these parameters in the equilibrium condition, the equilibrium time and constant parameters were removed from Eq.1.

Therefore, Eq.1 was rewritten as follows:

$$\psi = f_1(q.Y_t.H.\rho_s.\rho_w.\ g.d_{50}.\mu) = 0 \quad (2)$$

Where ψ represents the scour hole characteristics. Using Buckingham's theorem:

$$\frac{\psi}{H} = f_2\left(\frac{q}{\sqrt{gH^3}}.\frac{Y_t}{H}.\frac{d_{50}}{H}.\frac{\rho_s-\rho_w}{\rho_w}.\frac{\mu}{\rho q}\right) \quad (3)$$

The fluid viscosity effects (*Re*) on the scour hole characteristics could be neglected since the turbulent flow conditions were dominated on experiments (Mehraein et al. 2012). The $\frac{q}{\sqrt{gH^3}}$ referred to the Froude number on the weir crest. Further, by combining the dimensionless parameters $\frac{q}{\sqrt{gH^3}}$, $\frac{d_{50}}{H}$, $\frac{Y_t}{H}$ and $\frac{\rho_s-\rho_w}{\rho_w}$ a new dimensionless parameter $Fr_d = \frac{V}{\sqrt{g\ d_{50}\ (S-1)}}$ was obtained, in which S referred to the sediment particle density, V was the average fluid velocity calculated based upon the Manning equation $V = \frac{1}{n} R^{\frac{2}{3}} S^{\frac{1}{2}}$. Fr_d was the particle Froude numbers. Therefore, the last relationship of scouring was written as the function of the following dimensionless parameters:

$$\frac{\psi}{H} = f_3\left(F_r.\frac{Y_t}{H}.Fr_d\right) \quad (4)$$

in which $\frac{\psi}{H}$ represents the $\frac{L_d}{H}.\frac{h_d}{H}.\frac{L_0}{H}.\frac{L_s}{H}.\frac{d_s}{H}$.

4. Numerical model

4.1. Governing equations

Equations of fluid motion including continuity and momentum in three-dimension of the Cartesian Coordinate are as Eqs. (5) to (7).

$$V_F\frac{\partial\rho}{\partial t} + \frac{\partial}{\partial x}(\rho u A_x) + \frac{\partial}{\partial y}(\rho v A_y) + \frac{\partial}{\partial z}(\rho w A_z) = R_{DIF} \quad (5)$$

$$\frac{\partial u}{\partial t} + \frac{1}{V_F}\left\{uA_x\frac{\partial u}{\partial x} + vA_y\frac{\partial u}{\partial y} + wA_z\frac{\partial u}{\partial z}\right\} = \frac{1}{\rho}\frac{\partial\rho}{\partial x} + G_x + f_x - b_x \quad (6)$$

$$\frac{\partial v}{\partial t} + \frac{1}{V_F}\left\{uA_x\frac{\partial v}{\partial x} + vA_y\frac{\partial v}{\partial y} + wA_z\frac{\partial v}{\partial z}\right\} = \frac{1}{\rho}\frac{\partial\rho}{\partial y} + G_y + f_y - b_y \quad (7)$$

$$\frac{\partial w}{\partial t} + \frac{1}{V_F}\left\{uA_x\frac{\partial w}{\partial x} + vA_y\frac{\partial w}{\partial y} + wA_z\frac{\partial w}{\partial z}\right\} = \frac{1}{\rho}\frac{\partial\rho}{\partial z} + G_z + f_z - b_z \quad (8)$$

$$V_F\frac{\partial F}{\partial t} + \left(\frac{\partial}{\partial x}(FA_x u) + \frac{\partial}{\partial y}(FA_y v) + \frac{\partial}{\partial z}(FA_z w) + \frac{FA_x u}{x}\right) = 0 \quad (9)$$

Where V_F: the fractional volume opens to the flow, ρ: fluid density, R_{DIF}: a turbulent diffusion term. (u, v, w): flow velocity components in (x, y, z), (A_x, A_y, A_z): the fractional areas open to the flow in the directions (x,y,z), (G_x, G_y, G_z): body accelerations, (f_x, f_y, f_z): viscosity acceleration, and (b_x,b_y,b_z): flow losses in porous media. In Eq. (9), A: average of area flow and F is the fluid fraction. The F value was equal to the unit while the cell was full of the fluid, and zero while the cell was empty. According to Eq. (8) the volume of fluid (VOF) method was employed to track the free surface evolution. While the fractional area-volume obstacle representation (FAVOR) was employed to model fluid surface and rigid volumes such as geometric boundaries (Pourshahbaz et al. 2017; Khoshkonesh et al. 2019; Issakhov and Zhandaulet 2020; Shen and Zheng 2004).

The suspended load and bed load would be measured separately for the sedimentary computing part. The suspended load was acquired by solving the convection-diffusion transient equation (Eq. (10)).

$$\frac{\partial \mathrm{c}}{\partial \mathrm{t}} + \mathrm{U_i}\frac{\partial \mathrm{c}}{\partial \mathrm{xi}} + \mathrm{w}\frac{\partial \mathrm{c}}{\partial \mathrm{z}} = \frac{\partial}{\partial \mathrm{xi}}(\Gamma\frac{\partial \mathrm{c}}{\partial \mathrm{xi}}) \quad (10)$$

Where W: the sediment fall-velocity, Γ: diffusion coefficient. The coefficient of diffusion was proportional to the viscosity of the flow eddy and was determined by the k−ε model. Eq. (10) describes sediment transport including the effect of turbulence on the deceleration sediment particle settlement. Eq. (10) was solved on every cell except those near-bed which was implemented by the control volume method in the numerical model. Three models consisting of Van Rijn, Nielsen, and Meyer-Peter and Muller equations (Eqs. (11) - (13)) were developed to measure concentration and adjacent surface load (Wei et al., 2014; Bahmanpouri et al. 2020):

$$\boldsymbol{\varphi_n} = \mathbf{B_n}(\boldsymbol{\theta_n} - \boldsymbol{\theta_{cr.n}})^{\mathbf{1.5}} \quad \text{Meyer-Peter and Muller equation} \quad (11)$$

$$\boldsymbol{\varphi_n} = \mathbf{0.3}\ \mathbf{d_n}\ \mathbf{d_{*.n}^{0.7}}\left(\frac{\boldsymbol{\theta_n}}{\boldsymbol{\theta_{cr.n}}} - \mathbf{1}\right)^{\mathbf{0.5}} \quad \text{Van Rijn equation} \quad (12)$$

$$\boldsymbol{\varphi_n} = \mathbf{12}\ \boldsymbol{\theta_n}^{\mathbf{0.5}}\ \mathbf{B_n}(\boldsymbol{\theta_n} - \boldsymbol{\theta_{cr.n}}) \quad \text{Nielsen equation} \quad (13)$$

Where $\boldsymbol{B_n}$: the volume fraction of sediment particles, $\boldsymbol{\theta_n}$, $\boldsymbol{\theta_{cr.n}}$: Shields- and critical Shields parameter and $\boldsymbol{d_*}$: dimensionless particle diameter.

4.2. Description of the numerical model

The turbulence models including k−ε, k−w, the Renormalized Group (RNG) and large eddy simulation (LES) were employed to capture the turbulence characteristics. Sediment surface roughness

was defined by the bed roughness/d50 ratio which was about equal to one. The particle angle of repose which mostly depends on the bed angle with the typical magnitudes between 30 ° and 40 °, was measured and recorded as 33°. It was a useful term in correcting the slope's impact. The bed load coefficient regulated the bed load transport rate. According to Van Rijn (1987), the unit value was selected for the bed load coefficient. The scour rate was regulated by the entrainment coefficient which had a default value of 0.018.

4.3. Initial and boundary condition

At the channel inlet, the flow rate was considered as the boundary condition. Herein, the discharge of 0.01, 0.015, and 0.02 m^3/s with corresponded water elevation was applied. Walls on the sides, the bottom of the flume, and the flow rate at the flume outlet were considered as the other boundary conditions (Fig. 5). Boundaries of symmetry were also used at the upper boundaries. The hydrostatic pressure distribution was applied as an initial condition. Accordingly, various mesh cell sizes were examined to acquire the highest accuracy in reproducing the bed scouring processes. The mesh sensitivity analysis was conducted and based on statistical criteria of normal root mean square (NRMSE), the mesh size of 10.41 mm was applied for simulations (table 3). Indeed, the results of numerical simulations were compared with those obtained from the experiments (Eqs. (14) and (15)).

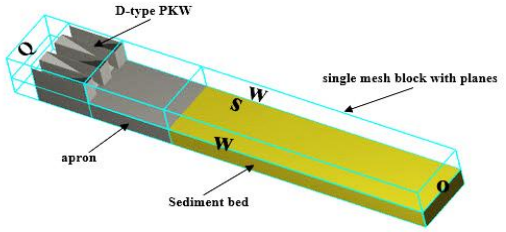

Figure 5. Scheme of boundary conditions of D-Type PKW

$$NRMSE = \frac{\sqrt{\frac{1}{n}\sum_{i=1}^{n}(obs_i - com_i)^2}}{obs_{i.max} - obs_{i.min}} \quad (14)$$

$$RE = \frac{(ds_{\max})_{exp} - (ds_{\max})_{num}}{(ds_{\max})_{exp}} \quad (15)$$

Where obs_i: observed experimental values, com_i: computational values, $obsi_{,max}$ and $obs_{i,min}$: the highest and lowest observed experimental values, n= number of data, $(ds_{\max})_{exp}$: the experimental maximum scour depth and $(ds_{\max})_{num}$: the numerical maximum scour depth. The *NRMSE* values between zero and 0.1 demonstrated high precision and between 0.1 and 0.2, 0.2 and 0.4 represented appropriate and average model precision, respectively (Khoshkonesh et al., 2019).

5. Results and discussion

5.1. Experimental results

Once the pump started, a vigorous scouring happened near the apron and a scour hole started to form. Herein, a rapid first phase followed by the development, stabilization, and, finally, a period of equilibrium. The first stage of the scouring could be defined as the most extreme stage of erosion capacity.

Breusers (1965) showed that at the beginning of the scour hole formation, some particles of the bed material were observed in suspension conditions near the upstream slope of the scour hole. Any of these suspended particles were transported within the main flow due to the internal equilibrium between the upward diffusive flux and the downstream flux. These particles would be deposited and suspended again due to the turbulent flow near the sediment bed. Further, several particles were transported as bed loads with the height of the jump lower than that of the reference height. The scouring depth increased considerably during the development process while the scour's hole shape remained the same. In this phase, the ratio of the maximum scour depth and the distance from the apron was almost constant. Hoffman (1998) based on experimental measurements revealed that the upper section of the upstream slope of the scour's hole was in equilibrium condition while the lower portion was continually expanding. The suspended load near the bed, which was associated with the conditions in the initial process, was decreased appreciably in the re-circulation region.

In the present study, the results showed that in the stabilization stage, the equilibrium condition was achieved for the upstream slope of the scour's hole as well as the scour depth. The process of equilibrium would be characterized as the stage in which no changes were observed in the dimensions of the scour's hole. The bed particles on the upstream slope of the scour's hole were rolling and sliding beneath the saltation height at this stage. The result is consistent with Hoffman (1998).

The characteristic parameters could be described as follows: a: scour depth near the apron and relative to the initial sediment level, ds_m: maximum scour depth, L_s: the horizontal distance of the location of maximum scour's depth from the apron edge, L_o: the horizontal extent of scour's hole from the apron edge, h_d: the dune height, and L_d: the horizontal distance of dune crest from the apron edge. The maximum scour's depth was the vertical distance from the initial level of the sediment bed to the deepest point of the scour hole profile. In particular, the discharge Q, water depth at upstream of the weir H_u and the tail water depth Y_t were considered as the parameters dominated the scouring processes (Table 2).

Table 2. measured and calculated parameters according to experimental and numerical results

Case	Weir type	Q (m^3/s)	H_u (cm)	t_{ad}* (hr)	Y_t (cm)	*dsm* (cm)		*Ls* (cm)		L_o (cm)		Relative error	*NRMSE*
						exp	num	exp	num	exp	num		
1	PKW5 D-Type	0.01	1.2	3	5	6.98	3.24	65	10	155	70	0.54	0.75
2		0.01	1.1	3	8	4.89	3.15	20	10	105	65	0.35	0.29
3		0.01	1.2	3	10	3.98	3.13	25	15	75	65	0.19	0.20
4		0.015	1.7	3	7	8.99	6.19	40	20	155	70	0.31	0.58
5		0.015	1.8	3	8.5	5.27	6.47	25	25	135	60	-0.22	0.26
6		0.015	1.5	3	10	5.10	5.53	20	20	125	55	-0.08	0.18
7		0.02	2.5	3	10	6.60	7.24	30	25	175	95	-0.09	0.82
8		0.02	2.5	3	12	5.46	8.43	25	25	135	65	-0.54	0.21
9		0.02	2.3	3	13.5	6.37	6.47	25	25	105	60	-0.01	0.12

*t_{ad}: time after water draining from flume

According to experimental observations (Fig. 6), the flow shear velocity at downstream increased with increasing the discharge Q resulted in washing the crest of the dune. Consequently, the washed material deposited at the end of the dune. Continuing this condition led to smoothing and longitudinal expansion of the dune surface. In some experiments, the sedimentary bed level was observed lower than the initial level of the bed. Further, the downstream wall of the scour hole was more affected by the variation in the discharge than the upstream wall. Similar findings were reported by Jüstrich et al. (2016) for linear and nonlinear weirs.

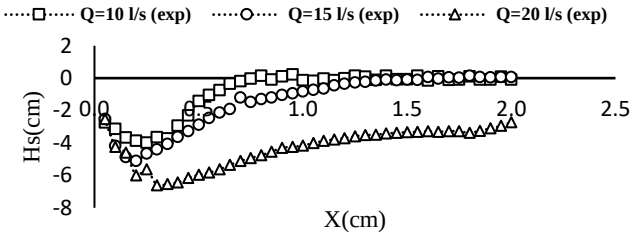

Figure 6. Effect of variation of discharge on scour hole in constant tail water depth (Y_t =10 cm)

Figure 7 shows the effect of tail water depth on scour hole at 3 different discharges, Q = 10 l/s (Fig. 7a), Q = 15 l/s (Fig. 7b) and Q = 20 l/s (Fig. 7c). In Figure 7a, which shows the variations of tail water depth on scour hole at flow depths of 5, 8, and 10 cm, it can be seen that the maximum scour depth increases with decreasing tail water depth. In the case of $\boldsymbol{Y_t = 5}$ cm, a decrease in tail water depth resulted in a decrease in dune height because the washed material was stratified on the bottom and did not form a dune. In Figure 7b, a high tail water depth resulted in reducing the maximum scour depth and its distance to the apron as well as the length of the scour hole. A dune bed form was originated at the downstream of the scour hole with the deposition of sediments that came out of the hole. The effective factor in the dune formation was the flow carrying capacity, which affected by the tail water depth, the water jet kinetic energy, and particle size. As can be seen in Fig. 7a-c reducing the tail water depth resulted in decreasing the dune height since the washed materials were layered on the bed and did not form a dune. The level of dune height in the D - type piano key weir was low so that in the downstream of the apron, there was practically no dune with a height similar to the dune height in linear weirs.

At the beginning of each test, a dune shape deposition was formed. When the flow condition did not allow the downstream dune height to increase further, the dune level was gradually flattered and the dune height was decreased until it finally aligned with the bed surface and in some experiments (with the low tail water depth) even reduced to less than the initial bed level.

After each test, scour profiles were measured using the point gauge when the water in the flume was drained out. The contours of the bed level after each test were plotted using Surfer software (Fig. 8). As seen, local scouring was variable in the transverse direction. It was due to geometric asymmetry of the channel, deviation of plunging jet from the top of the weir toward side walls, and then deviation toward the center, or secondary currents induced by hydraulic jump. Once the downstream depth was decreased the longitudinal place of the maximum scouring occurred at a farther distance from the apron. At Q=10 l/s, the longitudinal location of the maximum scour depth is 69.9 and 61.5% higher than the tail water depths of 8 and 10 cm, respectively, for a $Y_t = 5$ cm. Also, at Q=15 l/s, the longitudinal location of the maximum scour depth at $Y_t = 7$ cm is 37.5 and 50% farther from the apron than the tail water depths of 8.5 and 10 cm, respectively. In Q=20 l/s, the value of this parameter at the tail water depth of 10 cm is 16% higher than the tail water depths of 12 and 13.5 cm.

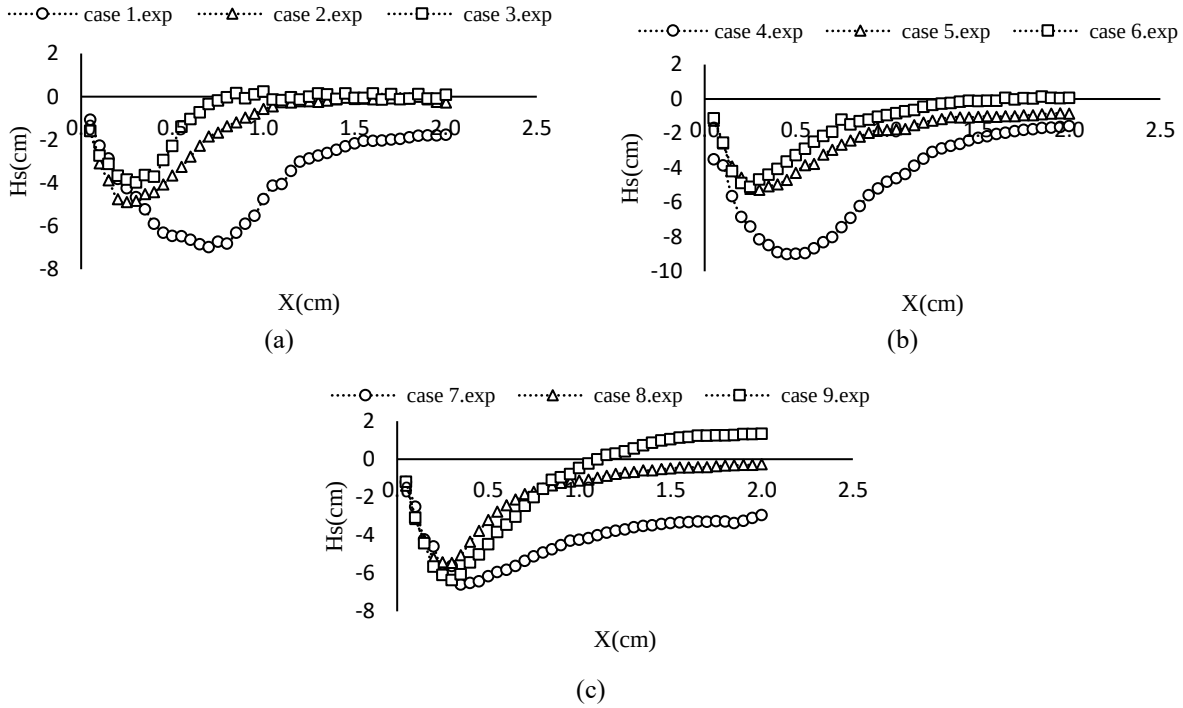

Figure 7. Effect of tail water depth on scour hole in constant discharge (a) *Q*=10 *l/s*, Y_t= 5, 8 &10 cm (b) *Q* =15 *l/s* and Y_t = 7, 8.5 and 10 cm (c) *Q* = 20 *l/s* and Y_t = 10, 12 and 13.5 cm

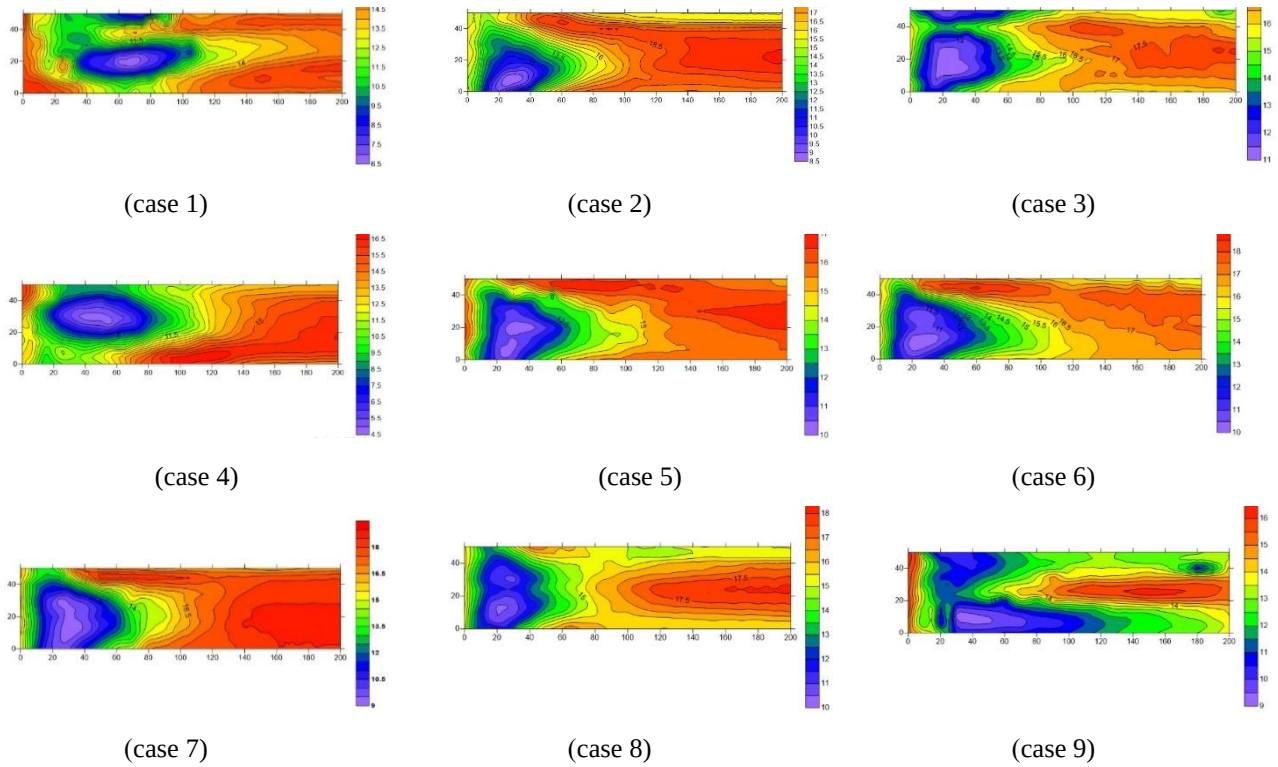

(case 1) (case 2) (case 3)

(case 4) (case 5) (case 6)

(case 7) (case 8) (case 9)

Figure 8. Contours of bed level after scour tests

5.2. Numerical results and discussion

In the current study, results of the local scouring downstream of D-type piano key weir was compared with numerical simulation results of the Flow-3D CFD model. According to laboratory tests, 18 numerical runs were conducted with the numerical model until achieving the steady flow condition associated with different running times (table 3).

While an Intel Core i7 2.5 GHz were employed for each simulation. In numerical modeling of hydraulic phenomena, one of the significant parameters in model calibration was the turbulence model to more accurately simulate the hydraulic phenomenon. Therefore, the turbulence models LES, RNG, k-ε and k-ω were evaluated. According to table 3 (simulations 6, 8, 9 and 10) it was observed that the LES had a about lowest NRMSE value than the other ones.

Furthermore, the maximum iterations in the LES model was roughly less than the others. Similar findings in terms of higher efficiency of LES turbulent model were reported by Yagmur et al. (2017) and Khoshkonesh et al. (2019), Nsom et al. (2019), and Khoshkonesh et al (2021) in reproducing the free surface flows and scouring processes.

Table 3. Characteristics of simulations performed in numerical model

simulation	Q (m^3/s)	Yt (cm)	Number of cells (*1000)	Mesh size (mm)	Turbulence Model	Bed load transport equation	simulation time (hr)	maximum number of iteration (N_i)	NRMSE
1	0.02	13/5	300	13.15	LES	Meyer-Peter & Muller equation	28	70246	0.16
2	0.02	13/5	400	11.9	LES	Meyer-Peter & Muller equation	34	72424	0.15
3	0.02	13/5	500	11.1	LES	Meyer-Peter & Muller equation	47	78109	0.15
4	0.02	13/5	600	10.41	LES	Meyer-Peter & Muller equation	54	79168	0.13
5	0.02	13/5	700	9.9	LES	Meyer-Peter & Muller equation	36	56914	0.17
6	0.02	13/5	600	10.41	LES	Nielsen equation	41	63492	0.12
7	0.02	13/5	600	10.41	LES	Van Rijn equation	49	79347	0.13
8	0.02	13/5	600	10.41	K-e	Nielsen equation	59	86125	0.26
9	0.02	13/5	600	10.41	K-w	Nielsen equation	54	78375	0.16
10	0.02	13/5	600	10.41	RNG	Nielsen equation	60	86492	0.27
11	0.01	5	600	10.41	LES	Nielsen equation	43	70917	0.75
12	0.01	8	600	10.41	LES	Nielsen equation	41	68348	0.29
13	0.01	10	600	10.41	LES	Nielsen equation	61	105881	0.20
14	0.015	7	600	10.41	LES	Nielsen equation	45	68357	0.58
15	0.015	8/5	600	10.41	LES	Nielsen equation	46	68453	0.26
16	0.015	10	600	10.41	LES	Nielsen equation	42	68555	0.18
17	0.02	10	600	10.41	LES	Nielsen equation	47	66821	0.82
18	0.02	12	600	10.41	LES	Nielsen equation	43	66663	0.21

Laboratory observations showed that there were two types of prevailing flow in the D-type piano key weir: a) the inlet key pulled the approaching flow towards itself and similarly to the sharp-crested weirs with the sloping body of the flow, from the input crest evacuation to downstream, b) the second pattern was formed on the output keys.

In this section, the flowing water through the outlet crest, like a jet, was discharged downstream of the key section slope. The output flow from the inlet keys hit the surface at the downstream of the apron and because of the existing tail water depth, it appeared in two formats a) as surface rotation due to the low tail water depth and b) as surface disturbance due to the high tail water depth. Ouamane and Lemperiere, (2006) reported the same flow pattern for water flow passing through a Piano Keys weir. Further, a small part of the flow deviated downstream and after colliding with the apron surface, created a weak rotating area below the input keys.

The flow pattern through the output key was much more complex than the inlet key. In that part of the weir, due to the intersection of the flow caused by the falling jets from the side crests with the upstream flow, the water depth increased and when the output flow entered the apron area as a falling jet, the rotation area was formed sharply in front of the output key (Fig. 9).

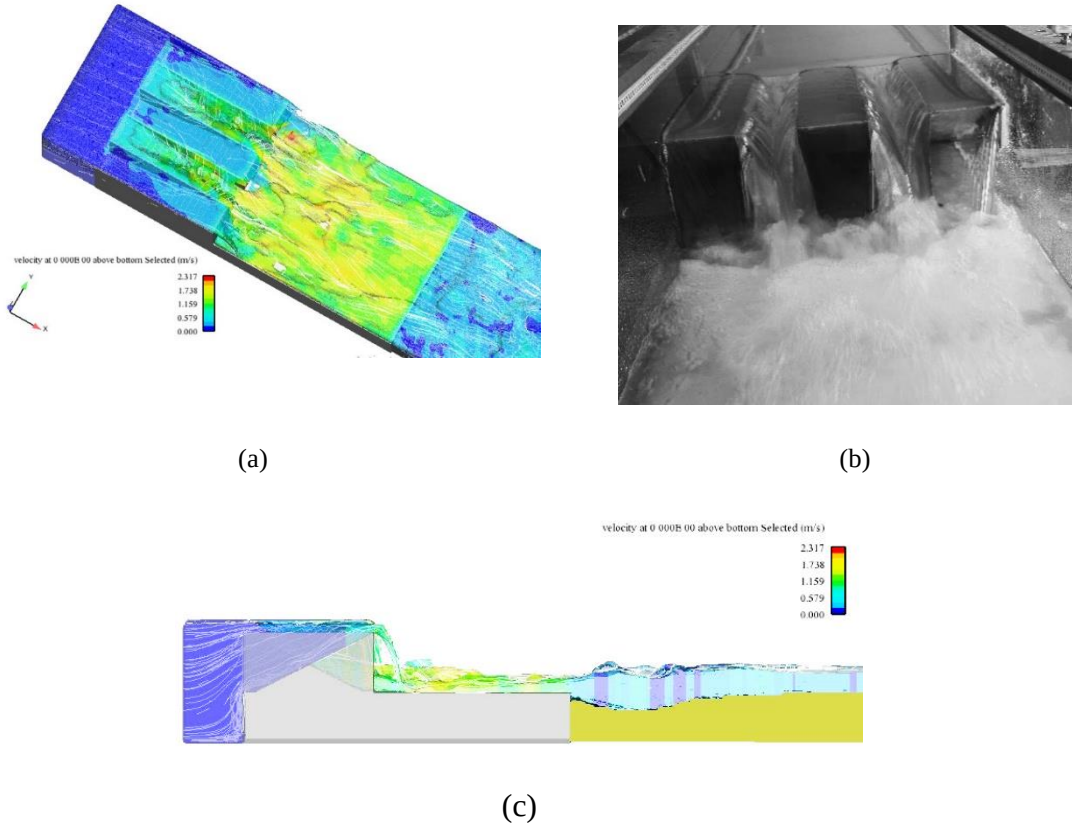

Figure 9. (a) Scheme of flow in physical model (b) Scheme of simulation in numerical model (c) The graphical output of the two-dimensional model of the position of the weir and the location of scour hole

For this reason, the bed sediments in front of the outlet key were washed more and removed from the flume sides. In the downstream of the apron, the scour hole occurred by the transmission of the flow crossing the bed. The starting point of the scour was immediately at the junction of the apron and the sediment. Over time, the scour hole dimension became larger and the jet transmission inside the hole changed to a rotating stream that helped to suspend some of the sediments by moving them downstream.

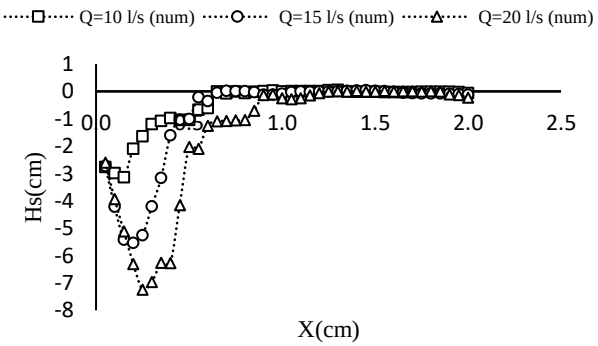

Figure 10. Effect of variation of discharge on scour hole in constant tail water depth (Yt= 10 cm) by numerical model results

Similar to laboratory results, the maximum scour depth increased with increasing the discharge rate from 10 to 20 l/s. The 3D schemes of the scour hole according to both experimental and numerical results are depicted in fig. 11. A good agreement between the numerical results and experimental data for the maximum scour depth and its distance from the apron is observed in fig. 11. Figure 12 shows the scour profiles based on the numerical model results. Comparing the profiles in Fig. 12 with Fig. 7, it can be seen that the numerical model performs well and the scour profiles show good agreement with the scour profiles obtained from laboratory results.

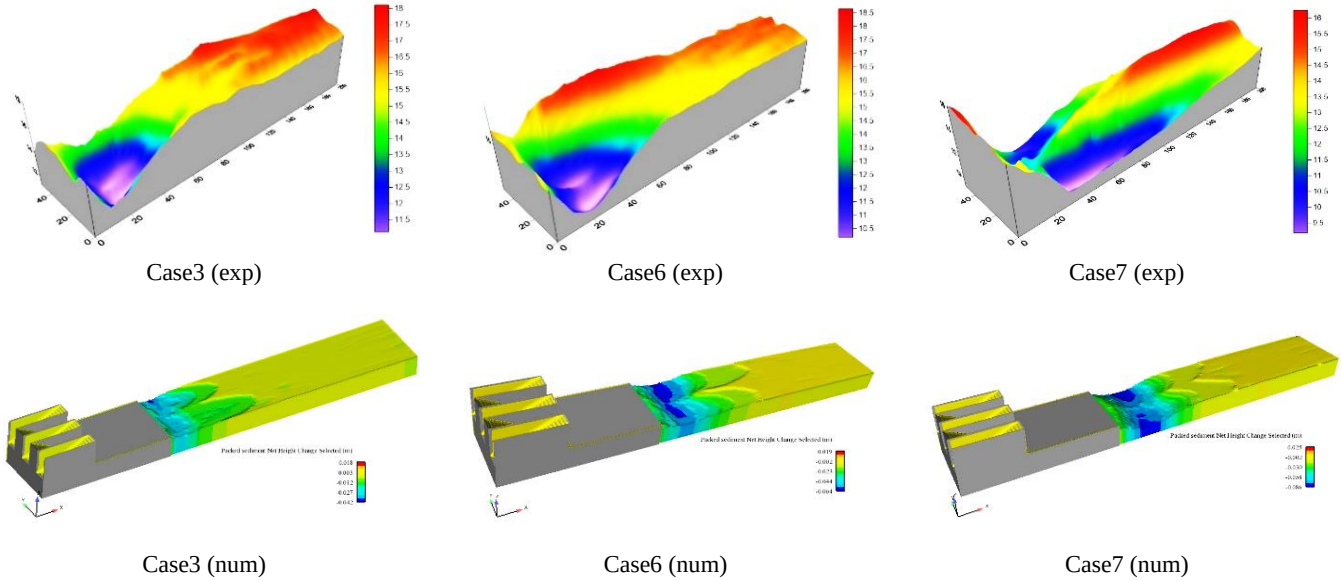

Figure 11. (a) 3D scheme of the scour hole in Surfer software using laboratory results (b) Numerical simulation results by numerical model

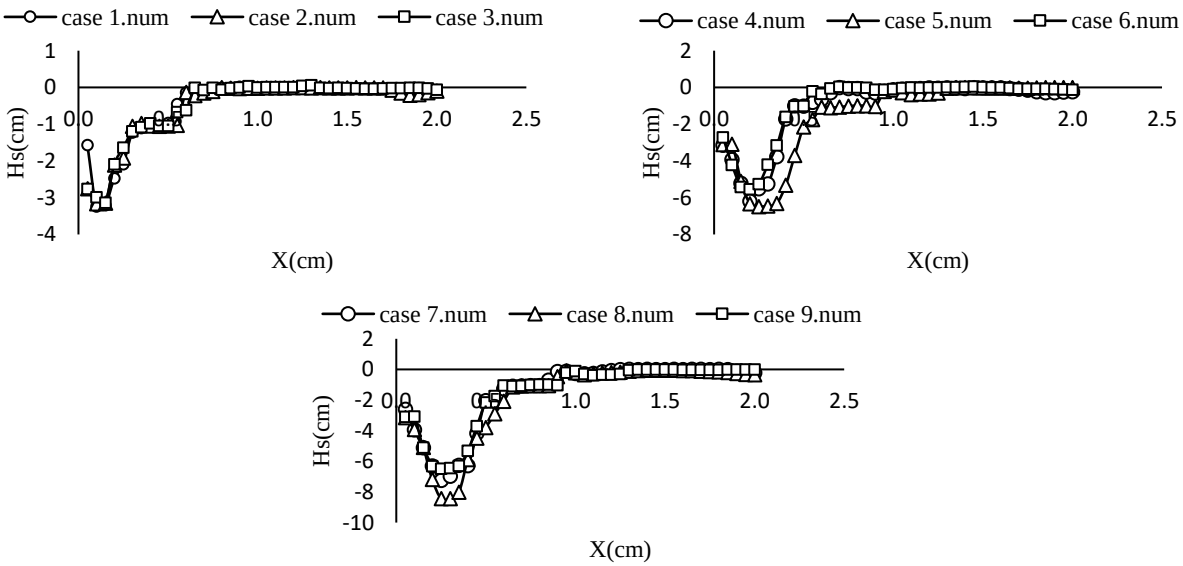

Figure 12. Scour profiles for different test cases

In the downstream of the weir, there was a large-scale re-circulating region which was developed (Fig 13). It was important to recognize that the re-circulation region resulted in a significant downward velocity component. The numerical results were consistent with the experimental data (Fig. 13 and Table 2).

As the outflow flow upstream of the weir crosses with the outflow flow downstream of the side crowns and increases the flow velocity, clockwise eddies are created at the base of the weir and a zone of flow rotation is created under the weir keys so that the scour downstream of the outlet keys is greater than the inlet keys. In general, it can be said that there is good agreement between the numerical and experimental results in terms of where the bed material begins to wash and that most of the sediment is washed near the apron

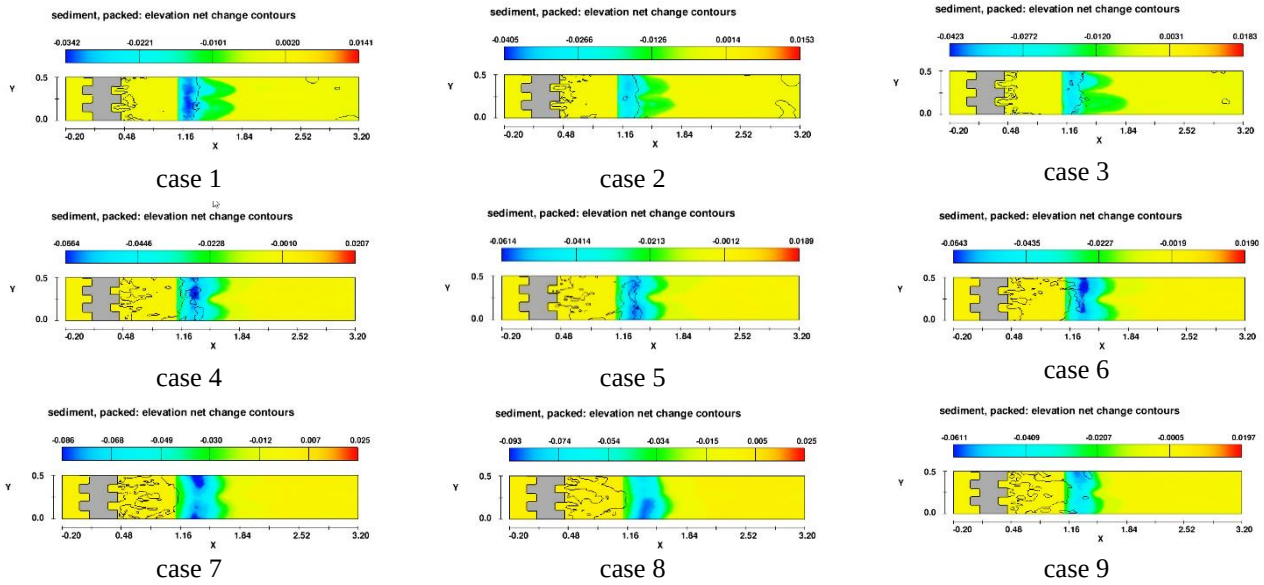

Figure 13. 2D scheme of bed level in the numerical model

Given that the discharge was one of the independent variables affecting the amount of scouring, a comparison between the maximum scour depth and its longitudinal place, as well as the greatest longitudinal expansion of the hole, is presented in fig. 14 (for different discharge rates with a constant tail water depth of 10 cm). As seen, the largest water depth increased with increasing the discharge rate for both experimental and numerical modeling. For the discharge rate of Q = 10 l/s, the maximum scour depth according to the experimental data was 3.98 cm while the numerical model predicted the maximum scour depth of 3.13 cm, which was 21% less than the experimental observation. For the discharge rate of the Q = 15 and 20 l/s, the maximum scour depth based upon the experimental data was 5.10 and 6.60 cm, respectively, however, the numerical results revealed the maximum scour depth of 8.4 and 9.7%, respectively. For Q=10 l/s, the longitudinal distance of the maximum scour position from the apron according to the experimental data was 25 cm, while, this distance based upon the numerical model was predicted 15 cm which was 40% less than the experimental observation. For Q = 15 l/s, both the experimental and numerical results depicted the same value of 20 cm as the longitudinal distance of the maximum scour position from the apron. For Q = 20 l/s, the longitudinal distance of the maximum scour position from the apron according to the experimental data was 30 cm, while, numerical results showed it was equal to 25 cm about 17% less than experimental observations. Overall, according to the numerical results, increasing the discharge rate led to increasing the distance of the longitudinal location of maximum scouring from the apron. With increasing the discharge rate, the flow capacity to carry out the sediment particles was increased. Further, the length of the scour hole increased with increasing the discharge rate in experiments, however, the numerical results didn't depict similar results. The length of scour's hole, decreased 15% with increasing the discharge from Q = 10 l/s to Q = 15 l/s, however, the scour hole length was increased with increasing the discharge to Q = 20 l/s. To protect the PKW, it is necessary to estimate the scour depth and its location. The length of scour hole indicates the location where it achieves the bed level. The prediction of this characteristic length allows designers to choose a length of bed that needs protection. Fig. 15 shows the dimensionless diagram of the characteristic of the scour hole.

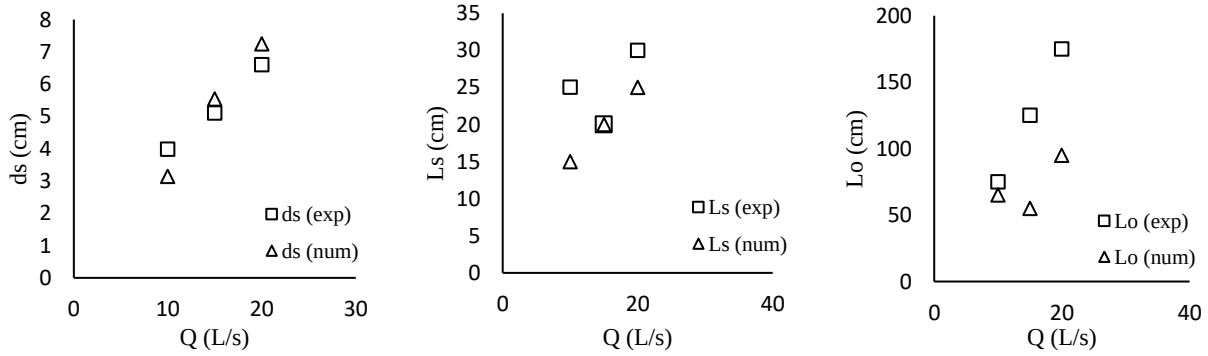

Figure 14. Comparison of characteristics of scour hole results using the experimental model and numerical model

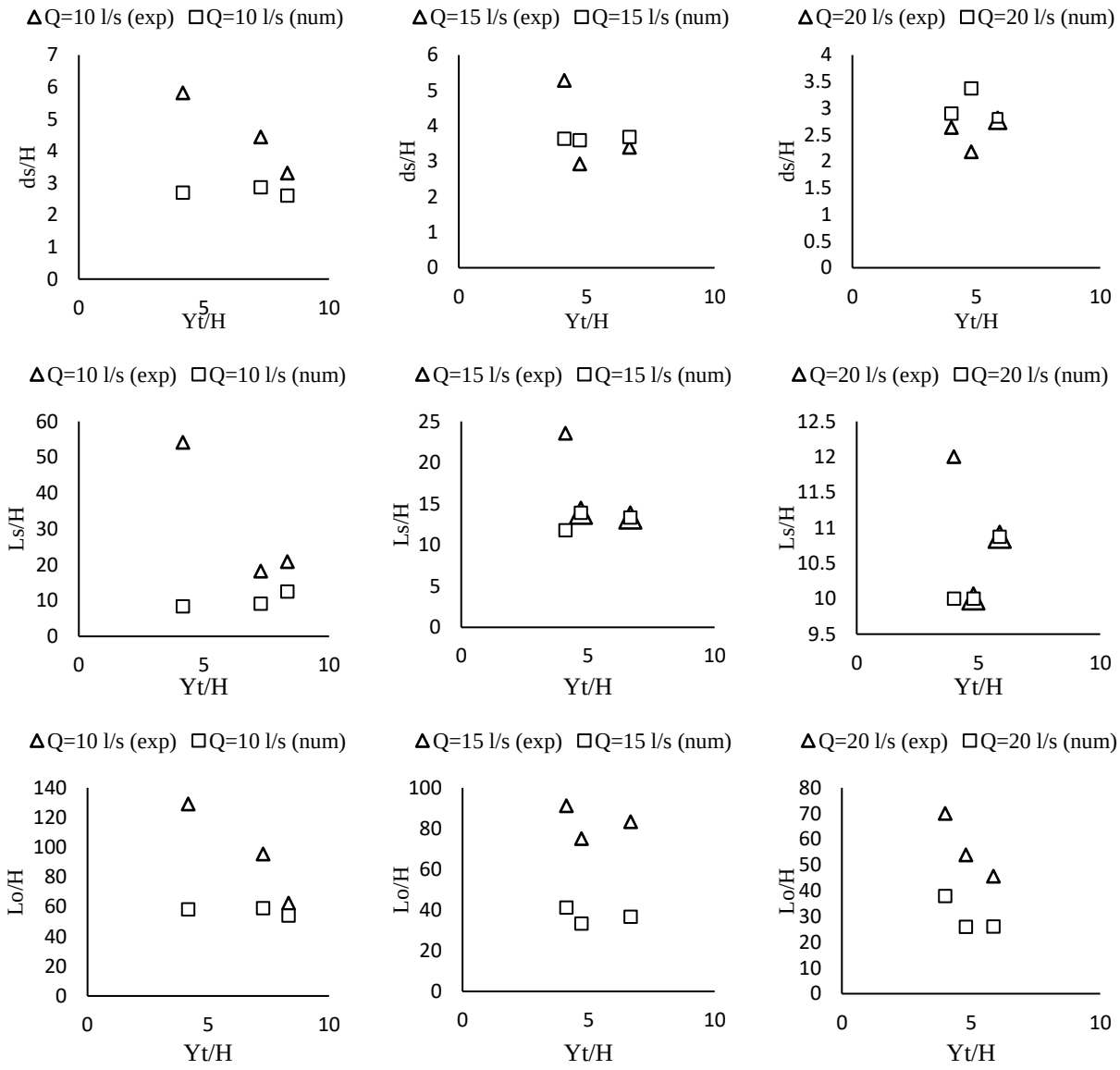

Figure 15. Dimensionless characteristics of the scour hole

The NRMSE value for Q = 10, 15 and 20 L/s were equal to 0.4, 0.3 and 0.3. The numerical model did not provide acceptable results when the tail water depth was reduced, which led to the error value was more than 0.5. The explanation was that the local bed-shear stress induced by the jet's high velocity exceeded the threshold bed-shear stress for the particle threshold of motion, resulted in local scouring downstream of the apron. For this reason, when the turbulence level increased and the free surface flow dissociated, the model was not able to accurately predict the scour mechanism. However, when the tail water depth increased and the turbulence level decreased, the numerical model estimated the scouring depth with acceptable quality and an error of less than 0.3.

6. Conclusion

The most critical parameter in the scouring process is the scouring depth. Aggregating eroded materials may affect the efficiency of dams and hydraulic structures. In the present study, as a first attempt, the maximum scour depth, downstream of the D - type piano key weir was investigated in terms of different discharge rates and tail water depths.

The results suggested that decreasing the water depth on the weir led to decreasing the jet velocity colliding with the downstream and the scouring rate was decreased. The scouring profile varied in the transverse direction and it was three-dimensional. Decreasing the downstream water depth resulted in increasing the maximum scouring depth and moving its longitudinal place toward downstream i.e. to the farther distance from the apron. Besides, increasing the discharge rate caused increasing the maximum depth of the scour hole, the longitudinal place of maximum scouring, and the length of the scouring hole. The results showed that LES resulted in a higher level of accuracy. The maximum scour depth was the parameter which simulated numerically with the highest rate of accuracy.

Acknowledgments

Authors would like to grateful to the Hydraulic Laboratory and the Computer Unit of Bu-Ali Sina University of Hamedan, Iran, for their technical assistance.

7. References

1. Bahmanpouri, F., Daliri, M., Khoshkonesh, A., Montazeri Namin, M., Buccino, M. (2020) Bed compaction effect on dam-break flow over erodible bed; experimental and numerical modeling, Journal of Hydrology.
2. Balachandar, R., Kells, J. A. (1997) Local Channel Scour in Uniformly Graded Sediments. Canadian Journal of Civil Engineering, 241(5), pp. 799–807.
3. Bhuiyan, F., Hey, R. D., & Wormleaton, P. R. (2007) Hydraulic Evaluation of W-Weir for River Restoration. Journal of Hydraulic Engineering, 133(6), pp. 596–609.
4. Bradley, J. N. Peterka, A.J. (1957) Hydraulic design of stilling basins. Journal of Hydraulic Division. 83. pp. 1-24.
5. Breusers, H. N.C. (1965) Conformity and Time Scale in Two-Dimensional Local Scour. Publocation 40, delft Hydraulics Laboratory, Delft, the Nether Lands.
6. Chatterjee, S. S., Ghosh, S. N., and Chatterjee, M. (1994) Local scour due to submerged horizontal jet. Journal of Hydraulic Engineering, 1208, pp. 973–992.
7. Dey, S., and Sarkar, A. (2006) Scour Downstream of apron Due to Submerged Horizontal Jets. Journal of Hydraulic Engineering, 132(3), pp. 246-257.
8. Dey, S. and Sarkar, A. (2007) Effect of Upward Seepage on Scour and Flow Downstream of apron Due to Submerged Jets. Journal of Hydraulic Engineering, 133(7), pp. 59-69.
9. Dietz, J. W. (1969) Kolkbildung in feinen oder leichten Sohlmaterialien bei stromen dem Abflub. Mitteilungen des theodor rehbok flubbaulaboratorium, Vol. 155, Universitat Fridericiana Karlsruhe, Karlsruhe, Germany, 1–122 in German.
10. Falvey, H. T. (2003) Hydraulic design of labyrinth weirs. ASCE Press (American Society of Civil Engineers) Reston, VA.
11. Faruque, M. A. A, Sarathi, P, & Balachandar, R. (2006) Clear Water Local Scour by Submerged Three-Dimensional Wall Jets: Effect of Tail water Depth. Journal of Hydraulic Engineering. 132(6), pp. 575-580.
12. Flow Science, (2010) FLOW-3D—User Manual Version 9.4. Flow Science.
13. Guan, D., Melville, B. W., & Friedrich, H. (2014) Flow Patterns and Turbulence Structures in a Scour Hole Downstream of a Submerged Weir. Journal of Hydraulic Engineering, 140(1), pp. 68–78.
14. Haffmans, G. J. C. M. and Pilarczyk, K. W. (1995) Local Scour Downstream of Hydraulic Structures. Journal of Hydraulic Engineering. 121(4). pp. 326-340.
15. Hoffmans, G. J. C. M. (1998) Jet scour in equilibrium phase. Journal of Hydraulic Engineering. 12(44), pp. 430–437.
16. Issakhov, A., & Zhandaulet, Y. (2020). Numerical study of dam break waves on movable beds for various forms of the obstacle by VOF method. Ocean Engineering, 209(March), 107459.
17. Jüstrich, S., Pfister, M., and Schleiss, A.J. (2016) Mobile Riverbed Scour Downstream of a Piano Key Weir. Journal of Hydraulic Engineering. 142(11).
18. Kabiri samani, A., and Javaheri, A. (2012) Discharge coefficients for free and submerged flow iver piano key weirs. Journal of Hydraulic Research, 50(1), pp. 114–120.
19. Karimi, M., Jalili Ghazizadeh, M., Saneie, M., & Attari, J. (2019) Experimental and numerical study of a piano key side weir with oblique keys. Water and Environment journal.
20. Khoshkonesh, A., Nsom, B., Bahmanpouri, F., Ahmadi Dehrashid, F., Adeli, A (2021). Numerical study the dynamic and structure of partial dam-break flow using VOF method. Water Resource Management, Springer, https://doi.org/10.1007/s11269-021-02799-2.
21. Khoshkonesh, A., Nsom, B., Gohari, S., Banejad, H. (2019) A comprehensive study on dam-break flow over dry and wet beds. Ocean Engineering, 188, 106279.
22. Kumar, B. and Ahmad, Z. (2020) Experimental study on scour downstream of a piano key weir with nose. Proceedings of the 8th IAHR International Symposium on Hydraulic Structures, ISHS 2020, (2019). doi: 10.14264/uql.2020.595.
23. Lempérière, F. and Ouamane, A. (2003) The Piano Keys weir: a new cost-effective solution for spillways. International Journal on Hydropower & Dams. 10(5), pp. 144-149.
24. Lemperiere, F. and Ouamane, A. (2006) Design of a new economic shape of weir. Dams and Reservoirs, Societies and Environment, 463-470.
25. Lempérière, F., Vigny, J.P., Ouamane, A. (2011) General comments on labyrinth and Piano Key weirs: The past and present" Proc. Int. Conf. Labyrinth and Piano Key Weirs Liège B, 17–24. CRC Press, Boca Raton, FL.
26. Li YL, Ma Y, Deng R, Jiang DP, Hu Z.(2019a) Research on dam-break induced tsunami bore acting on the triangular breakwater based on high order 3D CLSVOF-THINC/WLIC-IBM approaching. Ocean Eng. 182, 645-659. doi:10.1016/j.oceaneng.2019.03.067
27. Li YL, Yu CH (2019b). Research on dam-break flow induced front wave impacting a vertical wall based on the CLSVOF and level set methods. Ocean Eng. 178,442-462. doi:10.1016/j.oceaneng.2019.02.064
28. Machiels, O., S. Erpicum, B. J. Dewals, P. Archambeau and Pirotton, M.(2011) Experimental observation of flow characteristics over a Piano Key Weir. Journal of hydraulic research. 49(3), pp. 359-366.
29. Mehboudi, A., J. Attari and Hosseini, S. (2016) Experimental study of discharge coefficient for trapezoidal piano key weirs. Flow Measurement and Instrumentation. 50, pp. 65-72.
30. Mehraein, M., Ghodsian, M., Schileiss, A. (2012) Scour formation due to simultaneous circular impinging jet and wall jet. Journal of Hydraulic Research, 50(4), pp. 395–399.
31. Nsom, B., Latrache, N., Ramifidisoa, L. and Khoshkonesh, A. (2019). Analytical Solution to the Stability of Gravity-driven Stratified Flow of Two Liquids over an Inclined Plane. 24ème Congrès Français de Mécanique, Brest, 26 au 30 Août 2019. https://cfm2019.sciencesconf.org/244178/document.
32. Pagliara, S., Hager, W. H., F. ASCE and Minor, H. E. (2006) Hydraulics of plane plunge pool scour. Journal of Hydraulic Engineering, Vol. 132, pp. 450–461.
33. Pourshahbaz1, H, Abbasi, S., Taghvaei, P. (2017) Numerical scour modeling around parallel spur dikes in FLOW-3D. Journal of Drinking Water Engineering and science.
34. Rajaei, A. Esmaeili Varaki M. and Shafei Sabet, B. (2018) Experimental investigation on local scour at the downstream of grade control structures with labyrinth planform. Journal of Hydraulic Engineering, Published online: 05 Aug 2018.
35. Rajaratnam, N. (1981) Erosion by plane turbulent jets. Journal of Hydraulic Research. 19(4), Pp. 339-358.
36. Rajaratnam, N. and Macdougall, R. (1983) Erosion by Plane wall Jets with Minimum Tail water. Journal of Hydraulic Engineering, 109(7), pp. 1061-10.
37. Riberio, M. L., Pfister, M., Shleiss, A. J., and Boillat, J. L. (2012) Hydraulic Design of A-Type piano key weir. Journal of Hydraulic Research, 20(4), pp. 400–408.
38. Sarkar, A., and Dey, S. (2005) Scour hole downstream of aprons caused by sluices. Proc., Inst. Civ. Eng., Water Management J., London, 158June, 55–64.
39. Shen, Y. M., Ng, C. O., & Zheng, Y. H. (2004). Simulation of wave propagation over a submerged bar using the VOF method with a two-equation k-ε turbulence modeling. Ocean Engineering, 31(1), 87–95.
40. Van Rijn, L. C. (1987) Mathematical Modelling of Morphological Processes in the case of Suspended Sediment Transport. Hydraulics Communication No. 382.
41. Wei, G, Brethour, J., Grünzner, M., Burnham, J. (2014) The Sedimentation Scour Model in FLOW-3D. FSI-14-TN99.
42. Yagmur, S., Dogan, S., Hilmi Aksoy, M., Goktepeli, I and Ozgoren, M. (2017) Comparison of flow characteristics around an equilateral triangular cylinder via PIV and Large Eddy Simulation methods. Flow Measurement and Instrumentation, Vol. 55, pp. 23–36.
43. Yang, Y., Meilan Q., Xin, W., and Jinzhao Li. (2020). Experimental Study of Scour around Pile Groups in Steady Flows." Ocean Engineering 195: 106651.
44. Zhao, M., Cheng, L., Zang, Zh. (2010) Experimental and numerical investigation of local scour around a submerged vertical circular cylinder in steady currents. Coastal Engineering, Vol. 57, pp. 709–721.